Prediction of torsional failure in 22 cadaver femora with and without simulated subtrochanteric metastatic defects

A CT scan-based finite element analysis

Sander Spruijt[1], Jacqueline C van der Linden[1], P D Sander Dijkstra[2], Theo Wiggers[3], Mathijs Oudkerk[4], Chris J Snijders[5], Fred van Keulen[6], Jan A N Verhaar[1], Harrie Weinans[1] and Bart A Swierstra[7]

[1]Erasmus Orthopaedic Research Laboratory, Department of Orthopaedics, Erasmus MC, University Medical Center of Rotterdam, [2]Department of Orthopaedics, Leiden University Medical Center, Leiden, Departments of [3]Surgery and [4]Radiology, University Medical Center Groningen, Groningen, [5]Biomedical Physics and Technology, Erasmus MC, Rotterdam, [6]Faculty of Design, Engineering and Production, Delft University of Technology, Delft, [7]Department of Orthopaedics, Sint Maartenskliniek, Nijmegen, the Netherlands
Correspondence SS: s.spruijt@maartenskliniek.nl
Submitted 04-08-12. Accepted 05-05-16

Background **In metastatic bone disease, prophylactic fixation of impending long bone fracture is preferred over surgical treatment of a manifest fracture. There are no reliable guidelines for prediction of pathological fracture risk, however. We aimed to determine whether finite element (FE) models constructed from quantitative CT scans could be used for predicting pathological fracture load and location in a cadaver model of metastatic bone disease.**

Material and methods **Subject-specific FE models were constructed from quantitative CT scans of 11 pairs of human femora. To simulate a metastatic defect, a transcortical hole was made in the subtrochanteric region in one femur of each pair. All femora were experimentally loaded in torsion until fracture. FE simulations of the experimental set-up were performed and torsional stiffness and strain energy density (SED) distribution were determined.**

Results **In 15 of the 22 cases, locations of maximal SED fitted with the actual fracture locations. The calculated torsional stiffness of the entire femur combined with a criterion based on the local SED distribution in the FE model predicted 82% of the variance of the experimental torsional failure load.**

Interpretation **In the future, CT scan-based FE analysis may provide a useful tool for identification of impending pathological fractures requiring prophylactic stabilization.**

Prophylactic stabilization of impending pathological fractures is generally preferred over the surgical treatment of a manifest fracture (Dijkstra et al. 1994). The problem is to determine which metastatically involved bones require stabilization because of high fracture risk. Conventional guidelines for prophylactic stabilization of impending long bone fractures in metastatic bone disease remain controversial. Frequently cited guidelines are: a radiographic defect > 2.5 cm, and radiographic circumferential cortical destruction > 50% (Hipp et al. 1995). Unfortunately, these guidelines, as well as Mirels' scoring system (Mirels 1989), have proven to be insufficient (Hipp et al. 1995, Van der Linden et al. 2004).

FE analysis is a powerful tool for assessing the strength and failure load of bones (Keyak et al. 1998, Keyak 2001). FE models allow one to investigate the effect of changes in defect geometry and bone properties on bone strength and stiffness, which are difficult to create experimentally. This method is also of advantage in studying a range of loading conditions. FE models of bones that represent the individually unique geometry, as well as the local bone densities of bones in three dimensions, can be made using quantitative CT scans. Using this technique for assessment of fracture risk in non-metastatically involved proximal femora, strong positive correlations between experimen-

DOI 10.1080/17453670610046424

tally-measured and FE-predicted fracture load have been found (Keyak et al. 1998, Keyak 2001).

The purpose of our study was to determine whether patient-specific quantitative CT scan-based FE analyses can be used to predict fracture load and location in a cadaver model for metastatic bone disease. Metastatic defects commonly appear as transcortical holes in long bones (Hipp et al. 1990). These defects alter the distribution of stress and strain within the long bone, and dramatically reduce the torsional strength and torsional stiffness of long bones (Elias et al. 2000). We therefore combined experimental whole-bone torsion tests and CT scan-based FE analysis of human femora with and without simulated transcortical subtrochanteric metastatic defects. Whole-bone torsional stiffness and strain energy density were calculated by FE analysis and used to predict experimental torsional fracture load and fracture location.

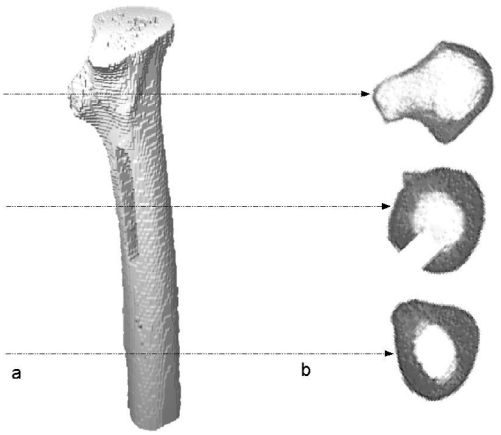

Figure 1. Three-dimensional model of the proximal part of a right femur from a 53-year-old female donor (a) and transverse cross sections (b). The model has an oblong simulated metastatic defect penetrating one entire cortex, with a defect length to bone diameter ratio of 200% in the subtrochanteric region. The elements were rectangular: 0.59 × 0.59 mm in the transverse plane and 2.0 mm in the longitudinal direction.

Materials and methods

In vitro experiments

11 paired fresh frozen human cadaver femora were obtained from 3 female and 8 male donors with a mean age of 70 (48–97) years. Radiographically, the femora showed no evidence of old fracture, metastasis, or other disease that could have affected their mechanical properties. All soft tissues were removed and the femora were frozen at –30°C. Before testing, the femora were thawed for 4 h at 21°C. Throughout the experiments, the bones were kept moist with 0.9% saline. In one randomly selected femur from each pair, a subtrochanteric medial defect was created to simulate a metastasis. The subtrochanteric region was chosen because almost 40% of impending and actual femoral pathological fractures are due to metastases located in this region (Dijkstra et al. 1994). The contralateral bone was left intact. Each defect was achieved by extramedullary drilling with progressively larger drill bits at low speed (800 rpm), to reduce the chance of damage at the edges of the defect. The defects were oblong with rounded ends and penetrated one entire cortex (Figure 1). This defect geometry was chosen because cortical defect length strongly influences the torsional strength of long bone (Hipp et al. 1990, Dijkstra et al. 1997, Elias et al. 2000, Hong et al. 2004, Van der Linden et al. 2004). We created 4 groups with longitudinal defects with defect length to bone diameter ratios of 50%, 100%, 150% and 200%. The defect width to bone diameter ratio was 25% in all cases. The median bone diameter at the center of the defect was 30 (27–32) mm, the median defect length was 31 (15–60) mm, and the median defect width was 8 (7–8) mm. This range of defect sizes falls within the current clinical guidelines, which state that a 2.5-cm defect with cortical involvement requires prophylactic stabilization (Hipp et al. 1995). It also covers the prospectively found risk factor of 30 mm longitudinal cortical destruction (Van der Linden et al. 2004).

The proximal and distal ends of each femur were embedded in aluminum molds filled with acrylate (2012 AB Araldite, Ciba, Switzerland). For better fixation, the femoral head was removed and 8 screws were used for both molds. The potted femora were mounted in a Zwick 1484 computer-controlled electrohydraulic testing machine (Zwick, Munich, Germany) and pure torsion was applied (Figure 2A). The moment of failure (Mexp), which was defined as the maximum moment achieved, was recorded. The location of the fracture was also recorded.

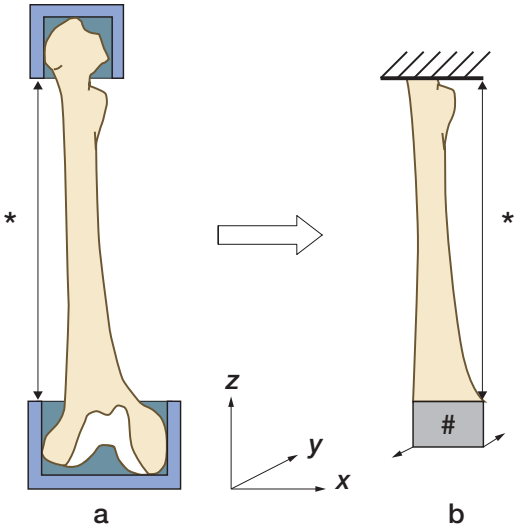

Figure 2. a. Experimental test configuration. The distal mold could move in the z-direction but could not rotate around the z-axis. The proximal mold could rotate around the z-axis, but could not move in this direction. By using ball-and-socket joints, both ends could rotate around the x- and y-axis. At the proximal mold, a force was applied to obtain pure torsion around the z-axis with a velocity of 5° per second.

b. Representation of the experiment in the FE model: the potted proximal bone-end was left out in the FE models. The length of femur in the models was representative of the non-embedded femoral length in the experiments (* = non-embedded length). The distal mold was modeled by a 24-mm thick block (#) with an elastic modulus of 200 GPa, to which the loads were applied to simulate the torsional load. All rotations and displacements at this end were left free. The most proximal slice of the model was fixed in all directions.

Quantitative CT

Before mechanical testing, the femora were CT scanned (Somaton Plus 4, Siemens AG, Erlangen, Germany) at 140 kVp, 146 mA, 1.5 seconds, 0.59 mm pixels, 512 × 512 matrix, together with a calcium hydroxyapatite calibration phantom (Kalender and Suess 1987). All femora were scanned using 2.0-mm thick slices. Since fracture of whole bones with lytic defects seems to depend on the minimum cross-sectional structural properties of the region encompassing the defect (Hong et al. 2004), the defect region was scanned contiguously. To reduce scanning time, the region above the defect was scanned at least every 4.0 mm and the shaft, which does not have large variance in its cross-sectional shape and density longitudinally, was scanned at 20-mm intervals. Two pairs of femora were scanned contiguously over their entire length.

Although the scanning intervals along the length of the bones differed, these differences are unlikely to have influenced the study results because data sets of femora that were not scanned contiguously were completed using software developed in-house. The bone geometry and density were interpolated to fill the space between the CT-scanned slices. This method was validated using the 4 contiguously scanned femora. Non-contiguously scanned data sets were created by selectively deleting CT slices from the contiguously-scanned femora. Subsequently, bone was interpolated in the deleted interval using the software. We calculated torsional stiffness for the contiguous models made directly from the scan data, and for models that were made using the interpolation method. The maximum difference between the contiguous and the interpolated models was less than 1%, which shows that the interpolated models are a good representation of the real bones.

Finite-element modeling and analysis

The finite-element models were made from the three-dimensional data sets from the quantitative CT scanner (Keyak et al. 1990, Weinans et al. 2000). The models consisted of brick elements of 0.59 × 0.59 × 2.0 mm and represented the actual geometry and bone density of the femora (Figure 1) . The bone mineral density of the elements was calculated from the calibrated CT attenuation. Elements with a density below 0.1 g/cm^3 were deleted, and bone elements with a density above 2.0 g/cm^3 density were assigned a density of 2.0 g/cm^3. The elastic modulus of each bone element was calculated from its bone mineral density using an experimentally determined relation (Carter and Hayes 1977). The bone tissue in the model was assumed to be linear elastic and isotropic. The number of elements of the 22 FE models ranged from 235,620 to 496,166.

We simulated the torsion experiment as follows. A block of elements with the mechanical properties of steel simulated the embedded distal bone-end in the experiment. The most proximal slice of the model was fixed in place (Figure 2b). Point loads were applied to the bottom of the simulated steel block to achieve a pure torsional load. Because the

models were linear, force magnitude was arbitrary. The deformation angle resulting from the applied torsional load was calculated using an iterative solver developed for this type of brick-model (van Rietbergen et al. 1996a), using a different Young's modulus for each element in the model (Weinans et al. 2000). The torsional stiffness (Sfe) was calculated by dividing the applied load by the deformation angle, and normalized for the bone length.

For each element, the strain energy density (SED) was computed from the stress and strain values that were calculated at the centroid of each element. This strain energy density is a scalar that represents the elastic energy stored per volume, and is calculated from the sum of the multiplication of the stress (σ) and strain (ε) components in all directions in each element ($\sum \sigma i\, \varepsilon i$). It is independent of the elastic modulus; however, the modulus distribution is of course the major variable that determines the energy distribution. To minimize the effect of the jagged surface of the modeled femora on the SED distributions, a post-processing filtration method developed for this type of FE model was used to smooth the data (Charras and Guldberg 2000). The area with the highest SED (SEDmax) in each femur was compared to the experimental fracture region. Four fracture regions were distinguished: fracture through the defect, fractures proximal to the defect, and fractures in the middle and distal third of the femur.

Statistics

The data are presented as mean (SD). To assess the ability of the FE models to predict torsional failure, simple linear regression analyses between experimental moment of failure (Mexp) and FE-calculated torsional stiffness (Sfe) were performed for femora with defects and without defects separately, and for the whole group. To test whether lumping of both groups was allowed, we performed a two-tailed Z-test. A null hypothesis was formulated, assuming that there was no difference between the regression coefficients of the regressions for the intact group and the defect group. A p-value < 0.025 was considered statistically significant.

In addition, simple linear regression analysis was performed between experimental moment of failure (Mexp) and maximum strain energy density (SEDmax) to determine the coefficient of determination (R^2). Multiple-variable stepwise linear regression was performed (F-to-enter ≥ 3.840, $p \leq 0.05$; F-to-remove ≤ 2.710, $p \geq 0.10$) to investigate whether the prediction of the Mexp improved when both Sfe and SEDmax were included in the regression. F-change was used for testing whether the inclusion of additional variables would result in a significant increase in R^2. Precision was described by the 95% confidence intervals (95% CI) for the regression coefficient of each regression line. All tests were performed using SPSS for Windows version 9.0 (SPSS Inc., Chicago, IL).

Experimental and FE-calculated fracture localizations

Femur pair	Intact group FEM	Intact group EXP	Defect group FEM	Defect group EXP
1	proximal	proximal	defect	defect
2	proximal	distal	defect	distal
3	distal	distal	defect	distal
4	proximal	proximal	defect	defect
5	proximal	proximal	defect	defect
6	distal	distal	distal	defect
7	middle	middle	defect	defect
8	proximal	distal	defect	proximal
9	proximal	middle	defect	defect
10	distal	distal	defect	defect
11	distal	distal	defect	defect

FEM finite element model, EXP experiment

Results

The mean experimental moment of failure, FE-predicted torsional stiffness and FE-calculated maximum SED were 131 (SD 50) Nm, 339 (122) Nm^2/radian, and 2.1×10^{-5} (2.0×10^{-5}) N/mm^2, respectively.

In general, the calculated locations of highest strain energy density matched reasonably well with the actual fracture locations in the experiments. For the entire group, the experimental fracture locations agreed in 15 of the 22 cases with the calculated location of the maximum strain energy density (Table). For the group with defects in 7 out of 11 cases, the maximum strain energy density locations fitted with the experimental fracture site. In the intact group, this was the case in 8 of 11 cases. Figure 3 shows an example of the calculated strain energy density distribution in a femur with a

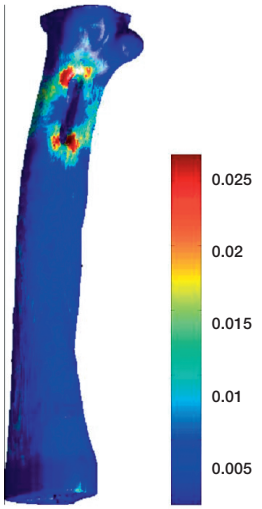

Figure 3. Typical strain energy density (SED, N/mm^2) distribution of a modeled right femur of a 53-year-old female. The highest SEDs around the subtrochanteric defect (defect length to bone diameter ratio of 200%) represent the onset of a fracture through the defect.

simulated metastatic defect. The peak strain energy density in this example is located at two corners of the generated defect.

When the intact and defect femora were analyzed separately, the FE model accounted for 80% and 76% of the variability in the experimental moment of failure, repectively (Figure 4). The two regression coefficients were not significantly different (Z = –0.92; p = 0.2), thereby justifying lumping of both data sets. For the total group, the calculated torsional stiffness in the FE model accounted for 72% of the variability in the experimental moment of failure, as shown in Figure 5.

The calculated maximum strain energy density value explained 68% of the variation in the experimental moment of failure (Figure 6). Multiple linear regression analysis demonstrated that FE-calculated torsional stiffness and maximal SED were significantly associated with experimental moment of failure, with a combined R^2 of 0.82 (F-change = 11.49, p = 0.003; Mexp = 0.22Sfe (95% CI: 0.10–0.34) -1.2×10^6SEDmax (95% CI: -1.9×10^6 to -4.5×10^5) + 81).

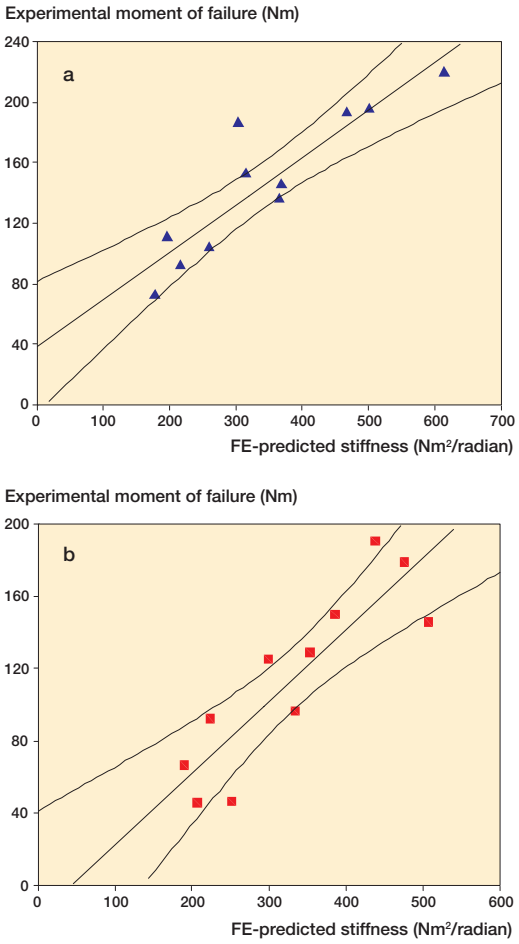

Figure 4. Experimental moment of failure (Mexp) plotted against the FE-calculated torsional stiffness (Sfe) and 95% confidence intervals for the regression are shown for (a) 11 intact femora (R^2 = 0.80, p < 0.001; Mexp = 0.313Sfe + 38.44, CI: 0.20–0.43) and (B) 11 femora with simulated metastatic defects (R^2 = 0.76, p < 0.001; Mexp = 0.397Sfe – 17.14, CI: 0.23–0.57).

Discussion

In this study, which we performed to validate our method, we have successfully demonstrated that CT scan-based FE analysis is capable of predicting the in vitro torsional fracture load (load-bearing capacity) of femora with and without simulated metastatic defects, regardless of defect size. We have also shown that linear models can be improved when the local strain energy distribution is taken into account. Clinical decisions as to prophylactic fixation should also take into consideration the

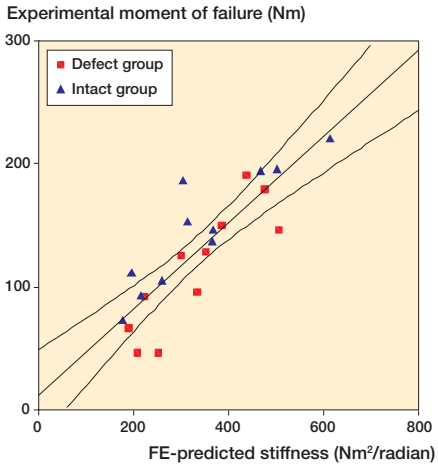

Figure 5. Scatter plot of experimental moment of failure (Mexp) versus the FE-calculated torsional stiffness (Sfe) for 22 femora with and without simulated metastatic defects (R^2 = 0.72, p < 0.001). The linear regression line (Mexp = 0.351Sfe + 11.78) and the 95% CI for the regression (0.25–0.45) are shown.

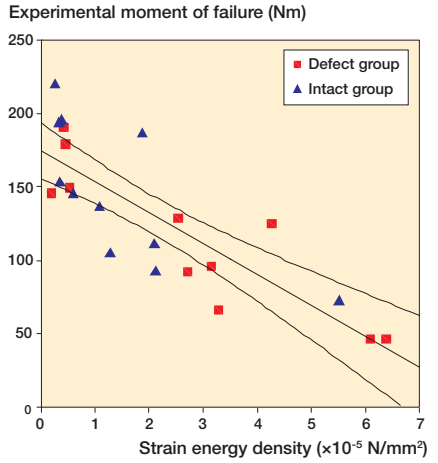

Figure 6. Scatter plot of experimental moment of failure (Mexp) versus the FE-calculated maximum strain energy density (SEDmax) for 22 femora with and without simulated metastatic defects (R^2 = 0.68, p < 0.001). The linear regression line (Mexp = -2.1×10^6SEDmax + 174.62) and the 95% CI for the regression (-2.8×10^6 to -1.4×10^6) are shown.

range of loads likely to occur in vivo (load-bearing requirements). Hipp et al. (1995) proposed a fracture risk ratio which is defined as the load-bearing requirement divided by the load-bearing capacity. When this ratio exceeds unity, fracture is likely. Based on data regarding loading conditions of the hip (Bergmann et al. 2001), it is possible to estimate the load applied to the femur during an index activity commonly incurred during daily living that may be associated with pathological fracture. The use of our FE models in combination with some load application criteria could in theory be used to automatically calculate the fracture risk.

The load-bearing capacity of a bone depends on both the material and the geometric properties of the entire bone. The strength of the predictive models in this study is that both geometric and material properties are incorporated automatically. This contrasts with the methods that are now commonly used in clinical practice for prediction of fracture risk. The latter methods rely on measuring the geometry of the metastatic defect alone, and therefore simply cannot provide an adequate structural assessment. An additional advantage of our technique compared to the prevailing methods is that it can predict fracture load regardless of defect size. Furthermore, it is a subject-specific technique—accounting for individual variations in bone geometry, density and loading conditions.

The routine use of CT scan-based FE analysis for every patient with a bone metastasis would be difficult to implement in clinical practice. A pragmatic approach could be to use the Mirels' (1989) scoring system as a screening tool for our technique. Since the system lacks specificity but has 100% sensitivity (Van der Linden et al. 2004), it is an ideal screening tool. Metastatic lesions tend to grow; thus, any method that predicts fracture risk for skeletal metastases is valid for only a finite period of time. To overcome this problem, we would recommend monitoring of the bone strength by periodically evaluating the Mirels' score and performing a quantitative CT scan-based FE analysis when indicated.

A potential source of error in the FE models is the jagged surface representation of the femora as a result of the use of rectangular elements. However, it should be noted that in a relatively fine mesh, as we used, the number of elements at the surface is relatively small compared to the number of elements in the entire mesh. In addition, we used a post-processing filtration method to improve the local solution accuracy (Charras and Guldberg 2000).

Another approximation is the use of isotropic material properties. In reality, bone tissue has a lamellar structure and is not isotropic, but good

correlations between FE-calculated stiffness and experimentally determined stiffness have been found using linear elastic isotropic material properties in computer models (Van Rietbergen et al. 1996b). Since there is no exclusive failure criterion established for bone, we have taken a pragmatic solution and have chosen the strain energy density in a filtered procedure using a post-processing filtration method (Charras and Guldberg 2000). Numerous other failure criteria for bone have been tried in the literature—based on stress, strain or strain energy (Keyak and Rossi 2000). All of these criteria concern scalars and have limitations in their ability to predict failure under various loading conditions. Recently, it has been shown that inclusion of an isotropic non-linear material representation in the model formulation can result in significantly improved FE predictions (Keyak 2001).

The specific load scenario that results in a pathological subtrochanteric fracture is unknown. Long bones are particularly weak in torsion, but considerably strong in bending (Miyasaka et al. 1991). Cortical defects significantly reduce long bone strength and stiffness, particularly for torsional loading (Hipp et al. 1989, 1990, Elias et al. 2000). With the types of defect proposed in this study, spiral fractures due to torsional loading often occur. The angular loading in this study provokes only this important mode of failure and represents a threatening loading component for long bones with metastatic defects. When applying the FE method to the clinical setting, more loading configurations (including bending and compression) should also be taken into account. Fortunately, our FE model permits superposition of multiple loading modes, making possible a more realistic representation of forces experienced in vivo in FE analyses.

The simulated lytic defects used in our experiment had idealized geometries with well-defined borders. Actual metastatic defects have more complex geometries, which were not studied here. However, more complex geometries can be studied using the same technique because they are automatically incorporated in the computer models made from the CT scans.

One potential limitation of this technique is that the presence of tumor(s) may alter the mechanical properties of bone within and adjacent to osseous metastases. However, there have been very few publications on this topic in the literature. Hipp et al. (1992) could not demonstrate whether the dependence of mechanical properties on trabecular bone density is altered by the presence of metastatic tumor(s). Others showed that metastatic trabecular bone has the same mechanical properties as normal trabecular bone, and that the density determined using quantitative CT can therefore be used to estimate the mechanical properties of trabecular bone in healthy and metastatically-involved bone (Kaneko et al. 2004). This contrasts with the findings of a similar study on cortical bone, where altered relationships between quantitative CT-measured density and mechanical properties were reported in the presence of tumor, compared with normal bone (Kaneko et al. 2003). Incorporation of these altered relationships in FE models may further improve the prediction of pathological fracture risk.

Our FE models correctly predicted the experimental fracture location in 15 of 22 cases, which is comparable to the results of a similar study (Keyak et al. 2001). Part of this relatively modest rate of agreement can be explained by the fact that our FE model could only predict the region of onset of fracture. In reality, fractures can begin in one region, stabilize thereafter, and then begin again in another region. Even so, this application of FE models further supports the usefulness of these models in studying pathological fracture risk.

In conclusion, we have demonstrated that CT scan-based linear FE analysis can be used for quantitative assessment of the in vitro load bearing capacity of human femora with and without simulated metastatic defects, regardless of defect size. We have thus created a validated research tool to investigate features that contribute to pathological fracture risk. Ultimately, this technique may identify patients with metastatic bone disease requiring prophylactic stabilization to prevent a pathological fracture more accurately than can be achieved using current guidelines.

Contributions of authors

SS conception and design of the study, FE-analysis, wrote and revised the manuscript. JCvL developed the FE-method, FE-analysis, contributed to the writing of the paper, reviewed and edited the paper. PDSD conception and design of the study, performed the experiments, contributed to the writing of the paper. TW conception and design of the study and

participated in the experiments. MO design of quantitative CT-scanning protocol, acquisition and post-processing of QCT data. CJS conception, design and supervision of the experiments. FvK participated in the experiments and development of the FE-methods. JANV conception and design of the study, reviewed and edited the paper. HW development of the FE-methods, contributed to the writing of the paper, reviewed and edited the paper. BAS conception and design of the study, supervised the study, wrote, reviewed and edited the paper.

The Dutch Cancer Society/Queen Wilhelmina Foundation supported this study through a research grant to Sander Spruijt, and Jacqueline van der Linden was supported by the Netherlands Organization for Health Research and Development (ZonMW). We thank Max Reijman for his advice regarding statistics.

Bergmann G, Deuretzbacher G, Heller M, Graichen F, Rohlmann A, Strauss J, Duda G N. Hip contact forces and gait patterns from routine activities. J Biomech 2001; 34 (7): 859-71.

Carter D R, Hayes W C. The compressive behavior of bone as a two-phase porous structure. J Bone Joint Surg (Am) 1977; 59 (7): 954-62.

Charras G T, Guldberg R E. Improving the local solution accuracy of large-scale digital image- based finite element analyses. J Biomech 2000; 33 (2): 255-9.

Dijkstra P D, Oudkerk M, Wiggers T. Prediction of pathological subtrochanteric fractures due to metastatic lesions. Arch Orthop Trauma Surg 1997; 116 (4): 221-4.

Dijkstra S, Wiggers T, van Geel B N, Boxma H. Impending and actual pathological fractures in patients with bone metastases of the long bones. A retrospective study of 233 surgically treated fractures. Eur J Surg 1994; 160 (10): 535-42.

Elias J J, Frassica F J, Chao E Y. The open section effect in a long bone with a longitudinal defect - a theoretical modeling study. J Biomech 2000; 33 (11): 1517-22.

Hipp J A, McBroom R J, Cheal E J, Hayes W C. Structural consequences of endosteal metastatic lesions in long bones. J Orthop Res 1989; 7 (6): 828-37.

Hipp J A, Edgerton B C, An K N, Hayes W C. Structural consequences of transcortical holes in long bones loaded in torsion. J Biomech 1990; 23 (12): 1261-8.

Hipp J A, Rosenberg A E, Hayes W C. Mechanical properties of trabecular bone within and adjacent to osseous metastases. J Bone Miner Res 1992; 7 (10): 1165-71.

Hipp J A, Springfield D S, Hayes W C. Predicting pathologic fracture risk in the management of metastatic bone defects. Clin Orthop 1995; (312): 120-35.

Hong J, Cabe G D, Tedrow J R, Hipp J A, Snyder B D. Failure of trabecular bone with simulated lytic defects can be predicted non-invasively by structural analysis. J Orthop Res 2004; 22 (3): 479-86.

Kalender W A, Suess C. A new calibration phantom for quantitative computed tomography. Med Phys 1987; 14 (5): 863-6.

Kaneko T S, Pejcic M R, Tehranzadeh J, Keyak J H. Relationships between material properties and CT scan data of cortical bone with and without metastatic lesions. Med Eng Phys 2003; 25 (6): 445-54.

Kaneko T S, Bell J S, Pejcic M R, Tehranzadeh J, Keyak J H. Mechanical properties, density and quantitative CT scan data of trabecular bone with and without metastases. J Biomech 2004; 37 (4): 523-30.

Keyak J H. Improved prediction of proximal femoral fracture load using nonlinear finite element models. Med Eng Phys 2001; 23 (3): 165-73.

Keyak J H, Rossi S A. Prediction of femoral fracture load using finite element models: an examination of stress- and strain-based theories. J Biomech 2000; 33 (2): 209-14.

Keyak J H, Meagher J M, Skinner H B, Mote C D, Jr. Automated three-dimensional finite element modelling of bone: a new method. J Biomed Eng 1990; 12 (5): 389-97.

Keyak J H, Rossi S A, Jones K A, Skinner H B. Prediction of femoral fracture load using automated finite element modeling. J Biomech 1998; 31 (2): 125-33.

Keyak J H, Rossi S A, Jones K A, Les C M, Skinner H B. Prediction of fracture location in the proximal femur using finite element models. Med Eng Phys 2001; 23 (9): 657-64.

Mirels H. Metastatic disease in long bones. A proposed scoring system for diagnosing impending pathologic fractures. Clin Orthop 1989; 249: 256-64.

Miyasaka Y, Sakurai M, Yokobori A T, Kuroda S, Ohyama M. Bending and torsion fractures in long bones (a mechanical and radiologic assessment of clinical cases). J Biomed Mater Eng 1991; 1 (1): 3-10.

van der Linden Y M, Dijkstra P D, Kroon H M, Lok J J, Noordijk E M, Leer J W, Marijnen C A. Comparative analysis of risk factors for pathological fracture with femoral metastases: results based on a randomised trial of radiotherapy. J Bone Joint Surg (Br) 2004; 86 (4): 566-73.

van Rietbergen B, Weinans H, Polman B J W, Huiskes R. Computational strategies for iterative solutions of large FEM applications employing voxel data. Int J Numer Meth Engng 1996a; 39: 2743-67.

van Rietbergen B, Odgaard A, Kabel J, Huiskes R. Direct mechanics assessment of elastic symmetries and properties of trabecular bone architecture. J Biomech 1996b; 29 (12): 1653-7.

Weinans H, Sumner D R, Igloria R, Natarajan R N. Sensitivity of periprosthetic stress-shielding to load and the bone density-modulus relationship in subject-specific finite element models. J Biomech 2000; 33 (7): 809-17.